https://doi.org/10.1016/j.tws.2023.110740

Predictive models for material properties of cold-formed conventional steels in the corner region

Haixin Liu [a], Junbo Chen [b, *], Tak-Ming Chan [a, c]

[a] Department of Civil and Environmental Engineering, The Hong Kong Polytechnic University, Hung Hom, Hong Kong, China

[b] School of Civil and Hydraulic Engineering, Huazhong University of Science and Technology, Wuhan, Hubei province, China

[c] Chinese National Engineering Research Centre for Steel Construction (Hong Kong Branch), The Hong Kong Polytechnic University, Hung Hom, Hong Kong, China

*Corresponding author: junbochen@hust.edu.cn

Abstract:

Current North American Specification AISI S100-16 provides design formulae to predict the yield strength of cold-formed steels. These design formulae were proposed on the basis of Karren's experimental works in 1967. The measured yield strength of the parent materials in Karren works only varies from 203 MPa to 315 MPa (29.5 ksi to 45.7 ksi). This paper aims to extend the validity of the design formulae to a wider range of material and geometry parameters, and a comprehensive material test program was carried out to further investigate the cold–forming effects. Nine batches of conventional steel plates were used, with the nominal thickness ranging from 2 mm to 5 mm and the nominal value of yield strength covering 235 MPa, 275 MPa and 355 MPa. A total of 81 flat coupons extracted from parent materials and 144 corner coupons sectioned from cold–formed corners were tested, with measured original yield strength up to 431 MPa and enhanced yield strength after cold-forming up to 625 MPa. These cold-formed corners were press-braked with different punch radii and included angles to achieve various geometric configurations which result in different levels of plastic deformation. The test data generated from this study were used in conjunction with data collected from the literature to establish a comprehensive database. Subsequently, predictive models were proposed to calculate the strength enhancements on the yield strength and ultimate tensile strength, and the loss in ultimate strain and elongation at fracture. It is shown that the proposed models can produce accurate predictions on the material properties of cold-formed steels.

Keywords: Strength enhancement; Predictive models; Material properties; Conventional steels; Cold–formed steels.

1. Introduction

Cold–formed structural steel members have been broadly used in a range of structural engineering projects as they offer merits of ease of fabrication, high strength–to–weight ratio, and economic efficiency. To achieve different design purposes, steel sheet materials can be cold–formed and further assembled into structural products with various shapes, including circular hollow section (CHS) [1], rectangular hollow section (RHS) [2], polygonal hollow section (PHS) [3, 4], single open section [5, 6], open built–up section [7, 8], and closed built–up section [9], etc. Two commonly used cold–formed manufacturing methods are cold–rolling and press-braking, in which the steel sheet is continuously fed into a successive set of rollers, or predetermined bends are punched along the length of the steel sheet, to produce required cold-formed steel sections. Both methods introduce different levels of plastic deformation into the deformed regions of cross–sections. As a result, the material properties of steels in the deformed region vary from those of parent materials due to the pronounced strain-hardening. A more rounded stress–strain response with enhanced yield strength and ultimate tensile strength and loss in ductility can be observed among those metallic materials experienced cold–forming. Generally, the change of material properties depends on the level of plastic deformation which can be further reflected by a measurable inner corner radius to thickness ratio of r_i/t [10].

Rasmussen and Hancock [11] and Dubina et al. [12] suggested that it is of significance to quantify the increasing strength in cold-formed steel structures resulting from cold work of forming. Also, for the calculation of overall cross-section resistance, the strength enhancement of cold-formed regions was well recognized in design standards such as Eurocode EN 1993–1–3 [13] and North American Specification AISI S100–16 [14]. Utilizing beneficial effects of cold-forming in cold-formed steel structure design is an important step towards achieving economic benefits. Hence, it is crucial to accurately determine the strength enhancement due to the cold-work, either by standard material tests or predictive models.

Karren [10] firstly proposed a semi-theoretical and semi-empirical strength enhancement model to relate the strength enhancement level with the plastic deformation level. The suitability of this semi-theoretical model has been proved and it has been extensively adopted to predict the strength enhancement of metallic materials. Van den Berg and Van der Merwe [15] modified the original Karren's model to predict the enhanced yield strength of different grades of stainless steels (EN 1.4003, 1.4016, 1.4301, 1.4401, and 1.4512) based on their test data and experimental results from Coetsee et al. [16]. Ashraf et al. [17] and Cruise and Gardner [18] both assessed the applicability of Karren's type predictive model, and proposed their predictive models respectively based on extensive stainless steel test results. These modified predictive models provided more accurate and consistent predictions on the enhanced yield strength for cold–rolled and press–braked stainless steel sections.

For structural carbon steels, Abdel–Rahman and Sivakumaran [19] found that the strength enhancement also exists in the vicinity of corners, based on the material test results on cold–formed steel channel sections, with a less level of enhancement as compared to those in the corner area. A modified Karren's model was then proposed to predict the average enhanced yield strength within the corner and adjacent enhanced area. Gardner et al. [20] calibrated the model coefficients against the test results on cold-rolled RHSs to provide a better prediction accuracy for the strength enhancement of cold-rolled RHSs. Rossi et al. [21] proposed an alternative model to predict the strength enhancement in the corner regions of cold-formed sections based on determining the plastic strains associated with the dominant stages in the fabrication process and using an inverted compound Ramberg-Osgood stress-strain relationship for the unformed material. Similarly, Pham et al. [22] conducted an investigation on the effects of the fabrication process on microstructure and material properties of cold-formed G450 channel sections, and proposed a modification to the original Karren's model to better predict the enhanced corner yield strength for this specific steel material. Based on the test results of 30 corner coupons extracted from cold-formed hexagonal hollow sections, Liu et al. [23] proposed a modified Karren's predictive expression to accurately predict the enhanced yield strength of Q690 high strength steels. It can be found that the aforementioned predictive models are established on the basis of corresponding databases covering a limited range of steel grades or limited range of r_i/t, and the applicability of these models to a wider range of steel grades and r_i/t needs to be further evaluated.

In this study, the effect of cold-forming and existing predictive models for strength enhancement of cold–formed steels are firstly reviewed. An experimental investigation on the cold–forming effect of nine batches of conventional steels was then conducted. A total of 81 flat coupons extracted from parent materials and 144 corner coupons machined from cold–formed angle sections were tested. The obtained material test results were further combined with collected data from literatures to form a fundamental database, covering a wide spectrum of normal strength steel grades, inner corner radius to thickness ratios, and included angles of corners. Subsequently, Karren's model [10] was re–

examined against the database, and further predictive models to calculate the ultimate tensile strengths, ultimate strains, and elongations at fracture after cold–forming were proposed.

2. Review on the cold–forming effect and the benchmark strength enhancement model

2.1 Mechanisms of the cold–forming effect

The mechanisms behind the variation of material properties after the cold–forming process are strain hardening and strain ageing of metallic materials. As illustrated in Fig. 1, during the yielding process of a steel specimen subjected to an external load, slip occurs between two adjacent planes of atoms, and the slip further generates a permanent deformation and random dislocation regions in the crystal structure. With the increase of deformation, the steel specimen gradually deforms into strain hardening range, in which more dislocations are generated and piled up between crystal boundaries and interactions between adjacent dislocations becomes more complicated, in turn restraining the slip and thus adding additional obstacles to the yielding process. At this moment, if the steel specimen is unloaded and reloaded immediately, higher proportional limit strength may be obtained, and the original ultimate tensile strength and remaining ductility will be conserved (shown as the green dash line in Fig. 1). This instantaneous effect of plastic deformation, known as strain hardening, leads to an increase in the proportional limit strength, but does not affect the ultimate tensile strength, and the original post-peak path preserves [24]. In the other case, if the deformed steel specimen is reloaded after sufficient time, the steel specimen behaves differently from the immediately reloaded counterpart. During the sufficient time before reloading, the foreign atoms, such as interstitial carbon and nitrogen atoms and other precipitations began to diffuse to the vicinity of dislocations, and subsequently fill the vacant space between dislocations. These impurities impede the movements and strengthen the interactions between dislocations [25]. This long–lasting effect is known as strain aging, which leads to an increase of the yield strength and ultimate tensile strength, but deterioration of ductility. Thereafter, increases in yield strength and ultimate tensile strength, but a loss in ductility can be observed in the test (shown as the red dash–dot line in Fig. 1). In general, the most significant part of strain aging effect happens in the first 14 days at ambient temperature or 30 mins at 100 °C [24, 26]. It should be noted that in this study enough elapsed time was allowed before material tests.

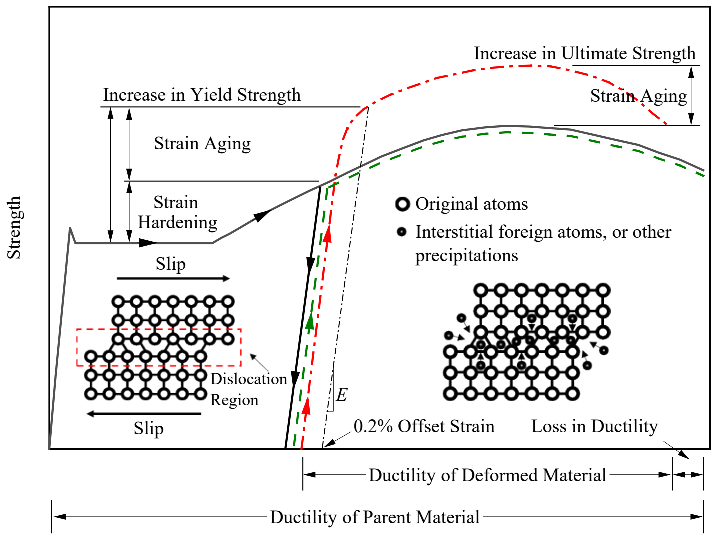

Fig. 1. Illustration for the effects of strain hardening and strain aging (modified from Chajes et al. [24]).

2.2 The benchmark strength enhancement model

In 1967, Karren [10] conducted a comprehensive experimental program, aiming at developing predictive models to relate the enhancement of yield strength with the plastic deformation experienced during cold–forming process. A semi–theoretical model has been proposed and calibrated on the basis of Karren's experimental data. To derive the final form of this semi–empirical predictive model, several simplifications and assumptions should be made as follows. A power equation was adopted to represent the strain hardening behavior of the plastic region in true stress–

strain response ($\overline{\sigma}-\overline{\varepsilon}$), as expressed in Eq. (1),

$$\overline{\sigma}=k\left(\overline{\varepsilon}\right)^{n_{\mathrm{se}}} \tag{1}$$

where k and n_{se} are material coefficient and strain–hardening exponent, respectively, as given in Eq. (2) and (3) [10],

$$k=2.80f_{\mathrm{u,f}}-1.55f_{\mathrm{y,f}} \tag{2}$$

$$n_{\mathrm{se}}=0.225f_{\mathrm{u,f}}/f_{\mathrm{y,f}}-0.120 \tag{3}$$

in which $f_{\mathrm{y,f}}$ and $f_{\mathrm{u,f}}$ are the yield strength and ultimate tensile strength of parent materials, respectively.

A simplified corner model was established to analyze the plastic strain caused by cold–works in the corner region, as shown in Fig. 2, in which t is the thickness of steel sheet, θ is the included angle, r_{i}, r_{n}, r_{o} are the inner corner radius, radius at the neutral surface, and outer corner radius, respectively. To theoretically compute the average corner yield strength $f_{\mathrm{y,c}}$ in the corner area, the effective stress was integrated over the entire area of the corner A_{c} using Eq. (1). The effective stress can then be integrated analytically, and the enhanced corner yield strength can be calculated by Eq. (4).

$$l_0 t f_{\mathrm{y,c}}=k\int_A\left|\overline{\varepsilon}\right|^{n_{\mathrm{se}}}dA \tag{4}$$

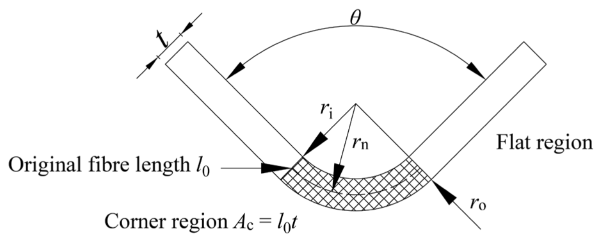

Fig. 2. Illustration of the simplified corner model.

Utilizing the assumptions of von Mises yield criteria under uniaxial tension and invariable volume strain of element, Eq. (4) can be subsequently converted to Eq.(5).

$$\frac{f_{\mathrm{y,c}}}{k}=\frac{1}{t}\int_{r_{\mathrm{i}}}^{r_{\mathrm{o}}}\left|\frac{2}{\sqrt{3}}\ln\frac{r}{\left(r_{\mathrm{i}}+r_{\mathrm{o}}\right)/2}\right|^{n_{\mathrm{se}}}\frac{r}{\left(r_{\mathrm{i}}+r_{\mathrm{o}}\right)/2}dr \tag{5}$$

If the ratio of r_{i}/t is less than 10, linear relationships can be found between $f_{\mathrm{y,c}}/k$ and r_{i}/t on the log–log figure, then Eq. (5) can be further simplified and approximated. The final form of Karren's predictive model can thus be obtained in Eq. (6),

$$f_{\mathrm{y,c}}=\frac{kb}{\left(r_{\mathrm{i}}/t\right)^{m}} \tag{6}$$

where b = 1.0-1.3n_{se} and m = 0.035+0.855n_{se}. This predictive expression of the enhanced yield strength $f_{\mathrm{y,c}}$ has been further standardized in American cold-formed steel members design specification [14] and Australian cold-formed steel structures design standard [27], with a rewritten form as expressed in Eq. (7).

$$f_{\mathrm{y,c}}=\frac{B_{\mathrm{c}}f_{\mathrm{y,f}}}{\left(r_{\mathrm{i}}/t\right)^{\beta}} \text{ in which } \begin{cases} B_{\mathrm{c}}=3.690\left(f_{\mathrm{u,f}}/f_{\mathrm{y,f}}\right)-0.819\left(f_{\mathrm{u,f}}/f_{\mathrm{y,f}}\right)^{2}-1.790 \\ \beta=0.192\left(f_{\mathrm{u,f}}/f_{\mathrm{y,f}}\right)-0.068 \end{cases} \tag{7}$$

3. Experimental investigation

An experimental program was conducted to investigate the material properties of conventional steels after cold–forming. In this program, a total of nine structural steel plates with three different nominal grades (Q235, Q275, and Q355) and three different thicknesses (2 mm, 3 mm, and 5 mm) were selected. Flat tensile coupons were firstly extracted from parent steel plates and tested to obtain material properties of parent metals. A series of steel plates were then press-braked into cold-formed angle sections and corner coupons were sectioned afterwards to investigate the effect of cold-forming.

3.1 Specimen details of flat coupons

To investigate the variations on material properties in different directions of parent materials, three flat tensile coupons were extracted from rolling, diagonal (45 degree), and transverse directions of parent steel plates, respectively, as shown in Fig. 3. In total, 81 pieces of flat coupons were fabricated in the experimental program. The flat coupon specimens were labelled by their nominal steel grades, thicknesses, and extraction directions. For instance, 275–3–D1 indicates that the first flat coupon extracted from the diagonal direction of 3mm Q275 plate.

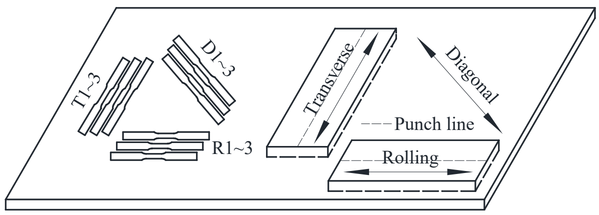

Fig. 3. Illustration of locations of flat coupons and different directions in parent steel plates.

3.2 Specimen details of corner coupons

All corner coupons were extracted from press–braked angle sections. To fabricate the press-braked angle sections, parent steel parent plates were firstly cut into small pieces with width by length of 120 mm × 400 mm, as shown in Fig. 3. Each small piece was subsequently press-braked into angle sections using a CNC press–braking machine. As the plastic deformation is associated with inner radius to thickness ratio r_i/t, punches with various punch radii (R_p = 3 mm, 5 mm, and 10 mm) were adopted and different included angles (θ = 90°, 120°, 135°, and 150°) were considered in the press-braking process, as shown in Fig. 4. Majority of steel plates were press-braked along the rolling direction, except for one batch of specimens on 5 mm Q355 plate, which was designed to be press-braked on the transverse direction, to consider the effect of directions of cold-forming on the change of material properties. After press-braking, the included angle of the angle sections was carefully measured by a digital protractor and the tolerance of the included angle is within ± 1°. It should be noted that geometric dimensions of press-braked angle sections in this study broadly covers the scope of application in North American Specification AISI S100-16 [14] ($r_i/t \leq 7$ and included angle $\theta \leq$ 120°), and no visible micro crack was observed in cold-formed regions after press–braking. Then two identical corner coupons were machined along the centerline of the corner in each press-braked angle section using a wire cutting machine. To ensure the repeatability and reliability of the test program, some repeated specimens were included. In this case, a total of four identical corner coupons were prepared.

(a) R_p = 3mm (b) R_p = 10mm (c) θ = 90°–150°

Fig. 4. Fabrication process and press-braked specimens.

The geometrical dimensions of flat and corner coupons were in line with the requirements of EN ISO 6892–1:2019 [28], while the dimensions and cross-sectional geometries of the corner coupon are shown in Fig. 5. It is worth noting that the width w of the parallel length is fixed as 5 mm for each corner coupon to ensure that the tested materials are included within the corner region experienced same amounts of plastic strains. To accurately measure the inner bending radius and area of curved coupons, the cross–section of the curved coupon was scanned and transferred into AutoCAD software to obtain corresponding inner curved radius and cross-sectional area. The specimens were named in a manner to identify the steel grade, nominal thickness, included angle and punch radius. For example, specimen 275–3–135–10 indicates a corner coupon extracted from a 135° angle section fabricated from the 3 mm Q275 steel plate using a punch with 10 mm punch radius. Totally, 144 pieces of corner coupons were fabricated in this experimental program.

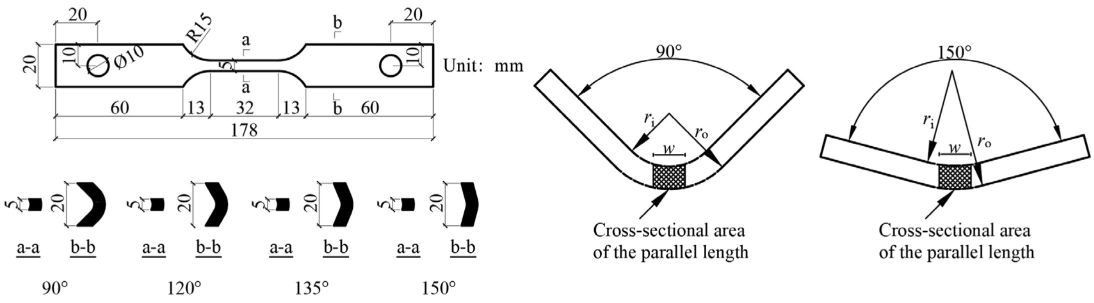

Fig. 5. Dimensions and cross-sectional geometries of the corner coupon.

3.3 Tensile test procedures

All tensile coupons were tested in accordance with EN ISO 6892-1:2019 using an Instron 100kN electromechanical testing machine, as shown in Fig. 6. A pair of uniaxial strain gauges with a gauge length of 5 mm were affixed to the center of both sides of the coupon to determine the Young's modulus. Young's modulus for each coupon was obtained through the linear regression of recorded stress over average reading of strain gauges between the range of $0.1f_y$ to $0.4f_y$. Full range of stress–strain responses of tested specimens were recorded with the aid of the inbuilt video extensometer. Several fine lines were marked perpendicular to the parallel length of coupons prior to the tensile tests following the approach adopted in Chen et al. [29]. After the completion of tensile tests, failed tensile coupons were matched together and the elongation at fracture was subsequently obtained by comparing the length after fracture to the original length. It is worth noting that the corner coupons were carefully aligned and tested using a specially designed pin grip to minimize the effect of eccentricity, while the flat coupons were tested using flat end clamps, as illustrated in Fig. 6.

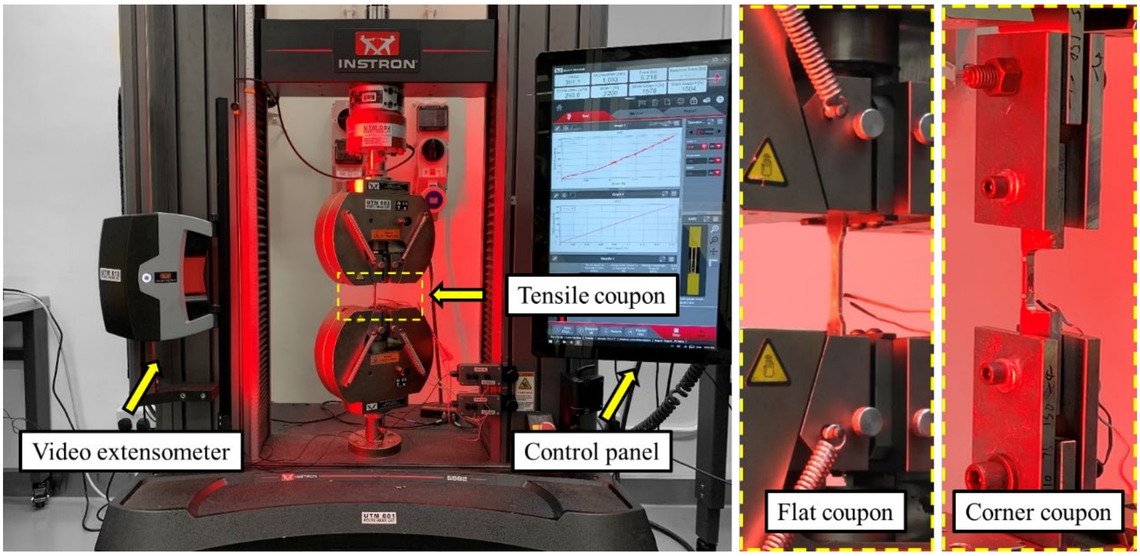

Fig. 6. Test setup.

In the coupon tests, displacement-controlled mechanism was adopted. The loading process was divided into three stages: initially a loading speed of 0.3 mm/min was used from the beginning to the end of yield plateau (or after 0.02% proof strength for corner coupons that have rounded stress-strain response), 0.8 mm/min up to ultimate tensile strength, and 2 mm/min until fracture of the specimen.

4. Experiment results and discussion

4.1 General

All material properties are tabulated at Table 1 and Table 2 for flat coupons and curved coupons, respectively, including the Young's modulus E, the yield strength f_y (taken as the lower yield strength for coupons with yield plateau or 0.2% proof strength for coupons without yield plateau), the ultimate tensile strength f_u, the ultimate strain ε_u (strain corresponding to f_u), and the elongation at fracture ε_f. Subscripts 'f' and 'c' are used to distinguish material properties of flat coupons and corner coupons, respectively. It can be found from Table 1 that material properties of flat coupons extracted from rolling, diagonal, and transverse directions of parent metals show little difference, indicating that the materials are isotropic. Apparent strength enhancements in not only the yield strength but also the ultimate tensile strength can be found among corner coupons. Stress–strain curves of all specimens are selected and presented in Fig. 7, in which colors of these curves are transitioning from black to red with the increase level of strength enhancement.

Table 1. Key parameters obtained from flat coupon tests.

Specimen		E_f	$f_{y,f}$	$f_{u,f}$	$\varepsilon_{u,f}$	$\varepsilon_{f,f}$	k	n_{se}	Specimen		E_f	$f_{y,f}$	$f_{u,f}$	$\varepsilon_{u,f}$	$\varepsilon_{f,f}$	k	n_{se}
–		(GPa)	(MPa)	(MPa)	(%)	(%)	–	–	–		(GPa)	(MPa)	(MPa)	(%)	(%)	–	–
235-2	R1	206.2	290	379	18.73	36.80	607	0.168	275-3	D3	208.7	331	486	16.32	31.52	792	0.173
	R2	208.0	284	376	18.58	40.50	592	0.160		T1	213.7	324	480	14.90	29.50	772	0.165
	R3	204.3	283	373	18.44	38.26	584	0.158		T2	210.1	327	479	14.90	23.65	789	0.177
	D1	202.6	287	365	18.89	40.53	576	0.160		T3	203.2	324	479	15.26	26.81	789	0.178
	D2	201.2	282	364	19.47	39.83	579	0.160	275-5	R1	214.7	328	452	17.45	33.50	673	0.133
	D3	202.9	282	364	19.31	41.86	577	0.158		R2	212.9	331	452	17.49	33.94	670	0.131
	T1	215.0	290	366	19.66	38.84	564	0.152		R3	217.0	336	453	16.93	33.33	665	0.153
	T2	212.5	299	368	18.80	35.73	563	0.152		D1	205.6	346	450	16.69	33.02	648	0.117
	T3	206.6	291	368	18.51	35.12	568	0.156		D2	210.7	343	451	17.11	36.32	655	0.122
235-3	R1	206.5	314	474	20.31	37.02	859	0.234		D3	212.2	342	450	17.03	38.93	654	0.121
	R2	212.1	303	465	21.57	38.27	850	0.240		T1	211.7	341	460	17.94	38.03	694	0.140
	R3	211.5	308	474	20.97	38.28	861	0.237		T2	212.5	345	452	17.40	41.58	663	0.126
	D1	210.8	313	463	21.75	40.50	838	0.234		T3	210.1	344	457	18.01	37.61	677	0.131
	D2	217.8	312	464	24.35	37.81	820	0.224	355-5a	R1	204.0	381	464	11.71	28.23	694	0.129
	D3	214.6	312	460	22.30	40.32	823	0.229		R2	204.5	379	463	13.35	30.12	693	0.131
	T1	213.7	312	467	19.43	31.61	806	0.208		R3	205.3	373	463	12.30	26.28	698	0.133
	T2	216.2	316	466	21.00	33.60	831	0.226		D1	199.8	380	463	10.83	25.07	686	0.125
	T3	212.2	319	463	20.10	32.38	831	0.229		D2	200.7	380	461	11.97	29.84	677	0.122
235-5	R1	202.9	307	465	21.28	38.71	833	0.229		D3	200.0	373	460	11.39	27.63	679	0.124
	R2	199.0	304	463	21.14	40.55	831	0.229		T1	205.0	383	466	11.68	26.93	684	0.122
	R3	204.0	302	463	21.15	38.84	832	0.229		T2	203.3	392	469	11.53	27.67	681	0.117
	D1	202.9	308	462	19.93	37.27	827	0.227		T3	207.0	391	472	11.49	28.97	693	0.122
	D2	206.9	310	463	20.21	37.11	824	0.225	355-5b	R1	194.6	390	535	18.43	36.72	939	0.214
	D3	206.5	305	460	20.15	36.61	824	0.227		R2	195.8	384	535	18.37	36.06	947	0.218
	T1	213.9	314	467	20.77	34.44	834	0.225		R3	200.7	384	533	19.00	36.10	941	0.217
	T2	211.9	317	465	19.75	32.00	831	0.226		D1	193.5	387	525	18.62	37.86	911	0.209
	T3	211.4	318	467	20.77	35.56	827	0.222		D2	189.2	382	525	18.33	33.27	913	0.209
275-2	R1	206.0	325	454	18.00	33.78	765	0.193		D3	186.5	385	524	18.06	33.90	920	0.214
	R2	178.5	334	455	18.08	34.98	753	0.185		T1	204.2	399	538	18.16	31.58	934	0.208
	R3	205.5	325	454	18.42	33.13	760	0.190		T2	205.9	396	538	18.10	32.25	941	0.211
	D1	199.3	335	446	18.30	32.99	738	0.185		T3	206.4	402	537	17.90	25.79	936	0.209
	D2	200.2	333	449	17.51	31.81	738	0.181	355-5c	R1	214.3	433	560	12.17	25.28	889	0.157
	D3	204.9	336	454	17.45	30.75	760	0.190		R2	212.9	430	559	12.17	20.99	888	0.157
	T1	207.0	335	456	17.28	32.84	768	0.191		R3	216.8	429	558	11.88	23.78	892	0.159
	T2	207.2	342	457	16.22	26.70	765	0.189		D1	205.7	426	549	12.88	28.44	873	0.158
	T3	206.7	337	460	17.82	30.82	765	0.187		D2	207.8	430	549	12.97	29.64	879	0.161
275-3	R1	217.3	328	483	16.26	32.83	801	0.182		D3	209.2	423	551	13.43	31.84	884	0.162
	R2	220.9	333	484	15.82	32.89	792	0.176		T1	198.4	415	549	14.18	31.38	876	0.161
	R3	215.6	333	486	16.55	34.39	801	0.179		T2	196.2	420	550	13.27	29.39	865	0.153
	D1	204.9	327	486	16.94	36.78	790	0.178		T3	199.9	416	547	13.37	31.67	871	0.159
	D2	207.1	332	487	16.44	35.46	791	0.173									

Notes: "R", "D", and "T" indicate the rolling, diagonal, and transverse directions, respectively.

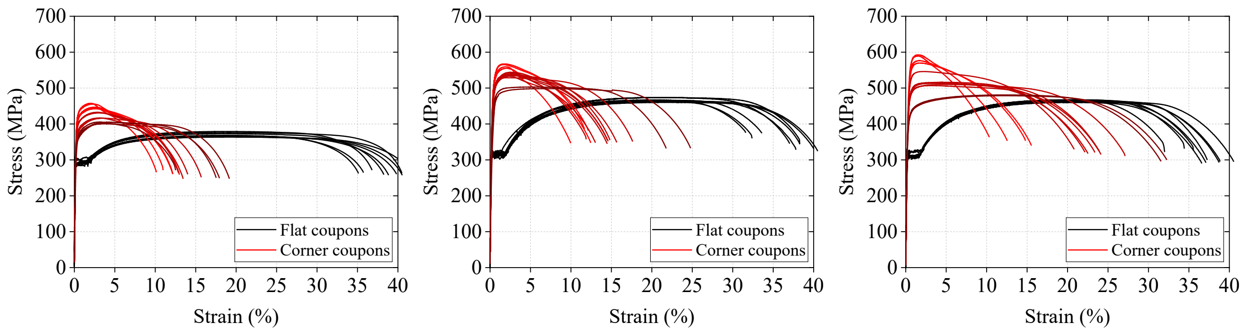

(a) 235 - 2 mm (b) 235 - 3 mm (c) 235 - 5 mm

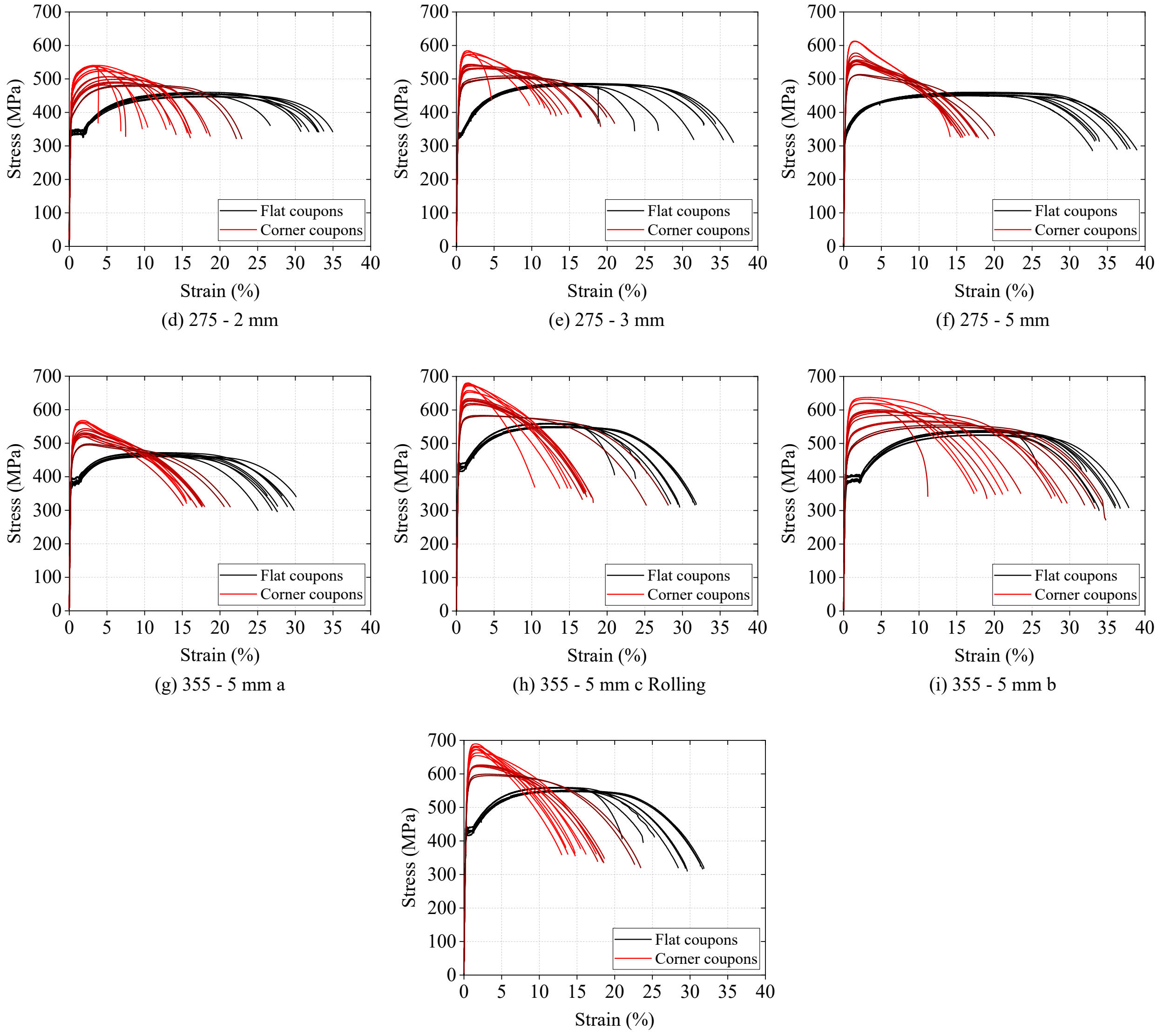

(d) 275 - 2 mm (e) 275 - 3 mm (f) 275 - 5 mm

(g) 355 - 5 mm a (h) 355 - 5 mm c Rolling (i) 355 - 5 mm b

(j) 355 - 5 mm c Transverse

Fig. 7. Stress-strain curves of tested coupons.

Table 2. Key parameters obtained from corner coupon tests.

Specimen –		r_i/t –	E_c (GPa)	$f_{y,c}$ (MPa)	$f_{u,c}$ (MPa)	$\varepsilon_{u,c}$ (%)	$\varepsilon_{f,c}$ (%)	Specimen –		r_i/t –	E_c (GPa)	$f_{y,c}$ (MPa)	$f_{u,c}$ (MPa)	$\varepsilon_{u,c}$ (%)	$\varepsilon_{f,c}$ (%)
235-2-90-3	-1	2.10	209.8	421	458	1.97	11.16	275-5-90-3	-1	0.61	190.8	558	612	1.52	13.71
	-2	2.11	208.0	420	455	2.33	12.07		-2	0.60	195.7	560	613	1.46	14.14
235-2-90-5	-1	2.65	207.0	408	443	2.52	13.40	275-5-90-5	-1	1.10	196.1	529	577	1.57	13.50
	-2	2.87	206.8	408	444	2.54	14.28		-2	1.08	189.5	521	568	1.64	14.64
	-3	2.92	201.9	406	442	2.56	13.34	275-5-90-10	-1	2.01	202.1	500	552	1.89	16.75
	-4	2.82	204.6	409	447	2.47	13.26		-2	2.05	195.5	492	543	1.96	16.29
235-2-90-10	-1	5.27	178.5	353	401	3.52	19.72	275-5-120-5	-1	1.19	191.2	504	551	1.66	13.75
	-2	5.44	205.7	363	405	3.10	13.76		-2	1.16	193.4	504	551	1.72	16.21
235-2-120-5	-1	3.34	205.3	391	431	2.95	15.42		-3	1.26	194.9	509	557	1.81	17.25
	-2	3.34	205.8	393	433	2.80	17.83		-4	1.27	192.5	507	554	1.66	16.14
235-2-135-5	-1	3.86	203.9	371	416	3.63	19.83	275-5-135-5	-1	1.40	194.9	506	553	1.67	15.82
	-2	3.65	208.3	376	417	3.06	18.44		-2	1.34	198.2	498	545	1.78	17.25
235-2-150-5	-1	4.69	206.7	351	405	4.45	21.83	275-5-150-5	-1	2.04	196.3	465	513	2.23	18.29
	-2	4.95	207.0	352	405	4.10	21.67		-2	2.14	195.5	467	512	2.06	19.21
235-3-90-3	-1	1.19	202.6	507	567	1.69	11.23	355-5a-90-3	-1	1.15	196.2	520	568	1.78	14.43
	-2	1.20	200.2	504	565	1.68	11.77		-2	1.11	193.1	513	563	1.90	14.32
235-3-90-5	-1	1.86	196.1	504	555	2.06	10.64	355-5a-90-5	-1	1.22	192.5	513	559	1.71	13.96
	-2	1.82	198.8	511	559	1.93	10.82		-2	1.29	197.6	516	563	1.72	13.57
235-3-90-10	-1	3.59	202.6	486	542	2.72	13.36	355-5a-90-10	-1	2.07	198.7	487	538	2.25	16.79
	-2	3.50	202.5	482	537	2.76	13.45		-2	2.06	198.6	496	543	2.12	14.61

	-3	3.54	204.1	483	539	2.68	14.36	355-5a-120-5	-1	2.26	195.1	481	525	2.18	17.14
	-4	3.44	203.8	487	544	2.55	12.91		-2	2.20	195.8	486	531	2.03	16.68
235-3-120-3	-1	1.79	197.0	475	535	2.37	16.00		-3	2.14	190.0	479	526	2.09	17.36
	-2	1.75	195.4	470	529	2.14	17.68		-4	2.10	197.9	483	530	1.97	18.93
235-3-135-3	-1	2.68	201.3	480	535	2.66	15.32	355-5a-135-5	-1	2.33	195.0	471	519	1.89	17.68
	-2	2.58	201.3	481	533	2.34	15.05		-2	2.35	195.6	475	520	2.12	17.29
235-3-150-3	-1	3.78	195.3	445	503	4.73	20.32	355-5a-150-5	-1	4.04	197.6	446	495	2.58	20.29
	-2	3.61	146.9	428	498	6.50	22.82		-2	3.84	201.1	446	498	2.69	20.75
235-5-90-3	-1	0.92	184.6	546	589	1.41	14.67	355-5b-90-3	-1	1.26	184.9	559	637	3.18	16.36
	-2	0.93	174.9	537	592	1.50	12.75		-2	1.28	186.1	553	632	2.93	17.25
235-5-90-5	-1	1.18	174.7	525	576	1.67	15.09	355-5b-90-5	-1	1.46	184.0	547	621	3.04	19.04
	-2	1.13	182.2	518	570	1.75	11.33		-2	1.37	185.8	546	620	2.81	18.32
235-5-90-10	-1	2.46	190.1	463	515	2.97	22.35	355-5b-90-10	-1	2.16	182.1	518	595	5.26	22.29
	-2	2.13	188.6	456	507	3.09	21.89		-2	2.19	188.4	520	600	4.44	20.79
	-3	2.31	189.9	460	513	3.55	19.51		-3	2.20	185.0	518	597	4.38	20.32
	-4	2.28	191.5	460	514	3.23	21.66		-4	2.14	186.6	521	597	3.72	19.57
235-5-120-5	-1	Tes data are unavailablet						355-5b-120-5	-1	2.42	182.2	502	584	6.50	25.21
	-2	1.67	187.1	496	546	2.26	18.01		-2	2.52	186.8	509	593	6.58	25.07
235-5-135-5	-1	2.14	186.1	466	516	4.26	19.81	355-5b-135-5	-1	3.46	187.5	472	564	9.81	26.96
	-2	2.14	186.9	457	510	4.86	25.08		-2	3.45	189.8	474	567	9.66	26.29
235-5-150-5	-1	3.21	183.9	408	479	11.84	30.41	355-5b-150-5	-1	5.31	186.8	438	549	13.31	30.79
	-2	3.53	185.4	411	481	12.54	29.30		-2	5.50	188.4	439	549	13.39	30.86
275-2-90-3	-1	2.20	203.1	479	540	3.21	11.89		-3	5.65	188.2	437	549	13.30	31.61
	-2	2.36	205.0	480	538	2.93	11.28		-4	5.72	188.3	442	555	13.10	33.46
275-2-90-5	-1	2.89	205.0	474	537	3.33	15.28	355-5cR-90-3	-1	0.96	184.8	613	681	1.50	12.94
	-2	2.76	204.9	475	539	3.36	14.50		-2	0.90	183.3	610	675	1.66	13.82
	-3	2.87	200.8	462	528	3.83	13.33	355-5cR-90-5	-1	1.03	182.6	607	672	1.74	13.02
	-4	2.89	205.0	477	540	3.91	16.00		-2	0.96	185.9	615	678	1.55	12.94
275-2-90-10	-1	5.57	198.7	412	482	4.61	1.83	355-5cR-90-10	-1	2.04	186.4	555	616	2.25	16.17
	-2	5.51	199.4	407	487	6.08	19.06		-2	2.04	184.1	560	619	2.16	17.36
	-3	5.37	199.1	417	499	6.16	18.61	355-5cR-120-5	-1	1.11	186.4	589	653	1.78	15.67
	-4	5.44	199.0	413	491	5.88	17.89		-2	1.09	188.3	594	658	1.75	15.21
275-2-120-3	-1	3.93	202.4	457	523	4.34	15.94	355-5cR-135-5	-1	1.17	192.9	566	628	1.89	17.66
	-2	3.67	204.0	457	524	4.49	16.83		-2	1.24	184.9	567	626	1.80	17.78
275-2-135-3	-1	4.75	202.5	431	506	5.13	18.00		-3	1.29	189.4	578	634	1.83	18.93
	-2	4.80	203.0	433	506	5.03	19.78		-4	1.30	186.4	571	630	1.91	17.66
275-2-150-3	-1	7.54	198.6	388	478	8.16	26.00	355-5cR-150-5	-1	1.68	188.9	525	581	3.89	24.08
	-2	6.72	200.9	390	482	8.60	25.78		-2	1.53	187.9	528	584	3.55	23.77
275-3-90-3	-1	1.09	197.8	522	580	1.72	12.14	355-5cT-90-3	-1	1.19	185.7	615	683	1.63	15.36
	-2	1.05	196.3	530	584	1.47	12.41		-2	1.12	184.8	606	673	1.70	15.40
	-3	1.02	191.2	516	573	1.86	12.68	355-5cT-90-5	-1	0.88	186.9	625	690	1.54	14.09
	-4	1.06	189.2	515	571	1.45	12.82		-2	0.92	184.2	617	681	1.76	13.21
275-3-90-5	-1	1.77	190.5	485	538	2.12	13.73		-3	0.94	181.0	609	673	1.45	15.13
	-2	1.81	186.1	478	531	2.72	17.18		-4	0.91	185.5	612	679	1.57	14.86
275-3-90-10	-1	3.60	188.8	440	502	7.04	21.23	355-5cT-90-10	-1	2.02	187.9	565	626	2.09	17.16
	-2	3.57	186.2	450	509	6.96	21.41		-2	1.99	189.3	567	627	2.32	18.09
275-3-120-3	-1	1.44	184.4	485	542	2.07	14.00	355-5cT-120-5	-1	1.34	186.3	598	663	2.02	18.01
	-2	1.36	186.6	492	544	1.78	15.45		-2	1.29	184.3	589	655	1.71	16.01
275-3-135-3	-1	1.61	190.8	472	530	2.97	16.82	355-5cT-135-5	-1	1.45	190.9	566	624	1.93	18.43
	-2	1.60	187.0	480	533	3.13	17.45		-2	1.44	186.2	560	622	2.11	19.08
275-3-150-3	-1	3.04	192.4	439	504	7.90	22.05	355-5cT-150-5	-1	1.99	190.6	537	595	3.47	22.58
	-2	3.21	186.5	439	503	7.72	23.64		-2	1.81	189.0	542	599	3.02	23.19

Notes: 355-5a, -5b, and -5c are three different types of steel plates with the same nominal grade of 355 MPa and the same nominal thickness of 5 mm. 355-5cR and 355-5cT are the plates extracted from the rolling and transverse directions of 355-5c parent materials, respectively.

4.2 Young's modulus E

As shown in Table 3, the average Young's modulus E_f of flat coupons of parent materials is 206.5 GPa, while the average E_c of corner coupons of cold–formed angles is 193.3 GPa. Fig. 8 illustrates that the Young's modulus is slightly reduced by 6.5% after cold–forming process when compared with the parent materials, indicating that plastic deformations may lead to degradation of Young's modulus of cold-formed steels. Similar observations have been reported in [30-32]. No apparent relevance between percentage of reduction and level of cold–forming can be observed.

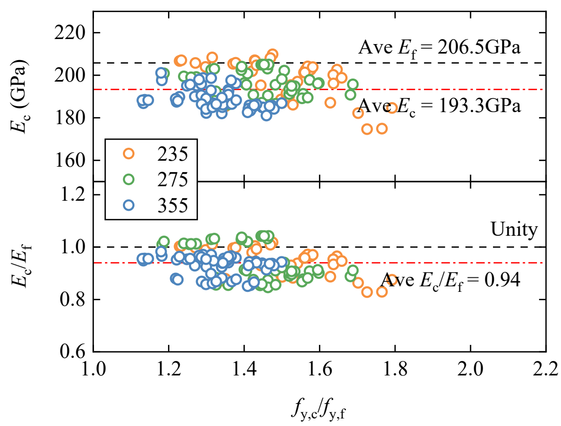

Fig. 8. Young's moduli E of tested corner coupons.

Table 3. Young's moduli of parent materials and cold-formed materials.

Specimen	E_f	E_c	E_c / E_f
–	GPa	GPa	–
Q235	209.1	197.1	0.943
Q275	209.2	195.7	0.935
Q355	203.4	188.8	0.928
Mean	206.5	193.3	0.935

4.3 Material coefficient k and strain–hardening exponent n_{se}

As incorporated in Eq. (1) to Eq. (6), material coefficient k and strain–hardening exponent n_{se} are two key parameters linking the predictive model to the material properties of parent materials. Hence, to obtain the k and n_{se} values, the engineering stress–engineering strain relations (σ_E–ε_E) of flat coupons were converted to true stress–true strain relations (σ_T–ε_T) through Eq. (8) and Eq. (9). And the true stress–true strain relations were then plotted on a log–log scale figure, as illustrated in Fig. 9 (a). The plots of the logarithm σ_T versus log ε_T appear as a straight line in the plastic region. Linear regression analysis is subsequently performed on plastic region following the approach in

Karren [10], utilizing a general regression equation of $\sigma_{\mathrm{T}} = k\varepsilon_{\mathrm{T}}^{n_{\mathrm{se}}}$. Data processing examples to obtain k and n_{se} values are given in Fig. 9 (b). The k and n_{se} values obtained from all flat coupon tests are tabulated in Table 1.

$$\sigma_{\mathrm{T}} = \sigma_{\mathrm{E}}(1+\varepsilon_{\mathrm{E}}) \tag{8}$$

$$\varepsilon_{\mathrm{T}} = \ln(1+\varepsilon_{\mathrm{E}}) \tag{9}$$

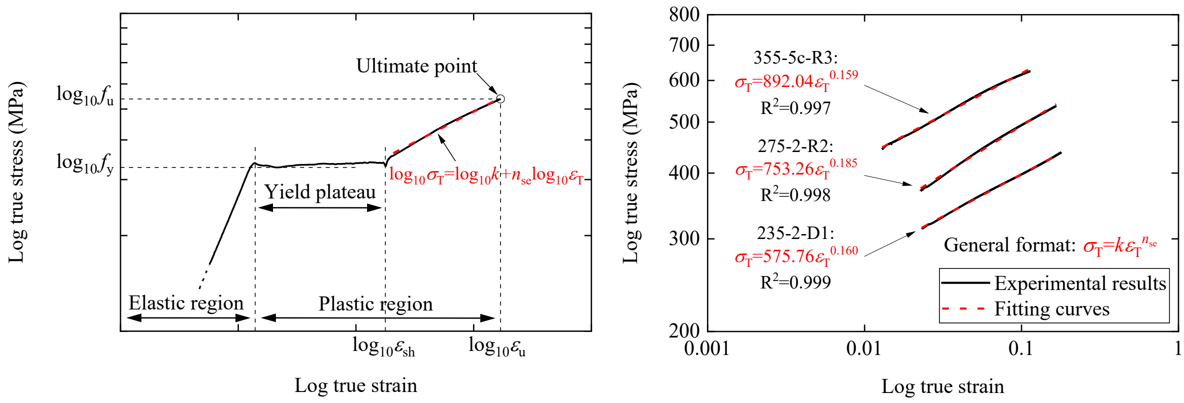

(a) Full range of stress–strain curve (b) Isolated plastic regions

Fig. 9. Example of obtainment of k and n_{se} values.

4.4 Strength enhancement due to the cold–forming effect

The level of strength enhancement for cold–formed steels is significantly associated with the level of permanent plastic deformation. In this study, the level of plastic deformation that specimens experienced directly relates to the adopted punch radius R_{p} and included angle θ during the press–braking process, and the level of cold–forming can be reflected by the measured r_{i}/t value of the corresponding corner coupon.

The obtained $f_{\mathrm{y,c}}$ and $f_{\mathrm{u,c}}$ of four representative groups of specimens are plotted against the included angle and punch radius in Fig. 10. General increase trends of strengths with increasing levels of cold–forming can be observed. For specimens press-braked by the same punch, a smaller included angle results in a larger plastic deformation and therefore a larger strength enhancement. For specimens with the same included angle (taking 90° as example) but press-braked by different punches, it is obvious that a smaller punch radius leads to larger plastic strains developed in the corner region, also resulting in a higher strength enhancement. It is also worth noting that the effects of different directions on the material properties of cold–formed steels are negligible, reflected by the test results of 355–5cR and 355–5cT specimens as displayed in Fig. 10.

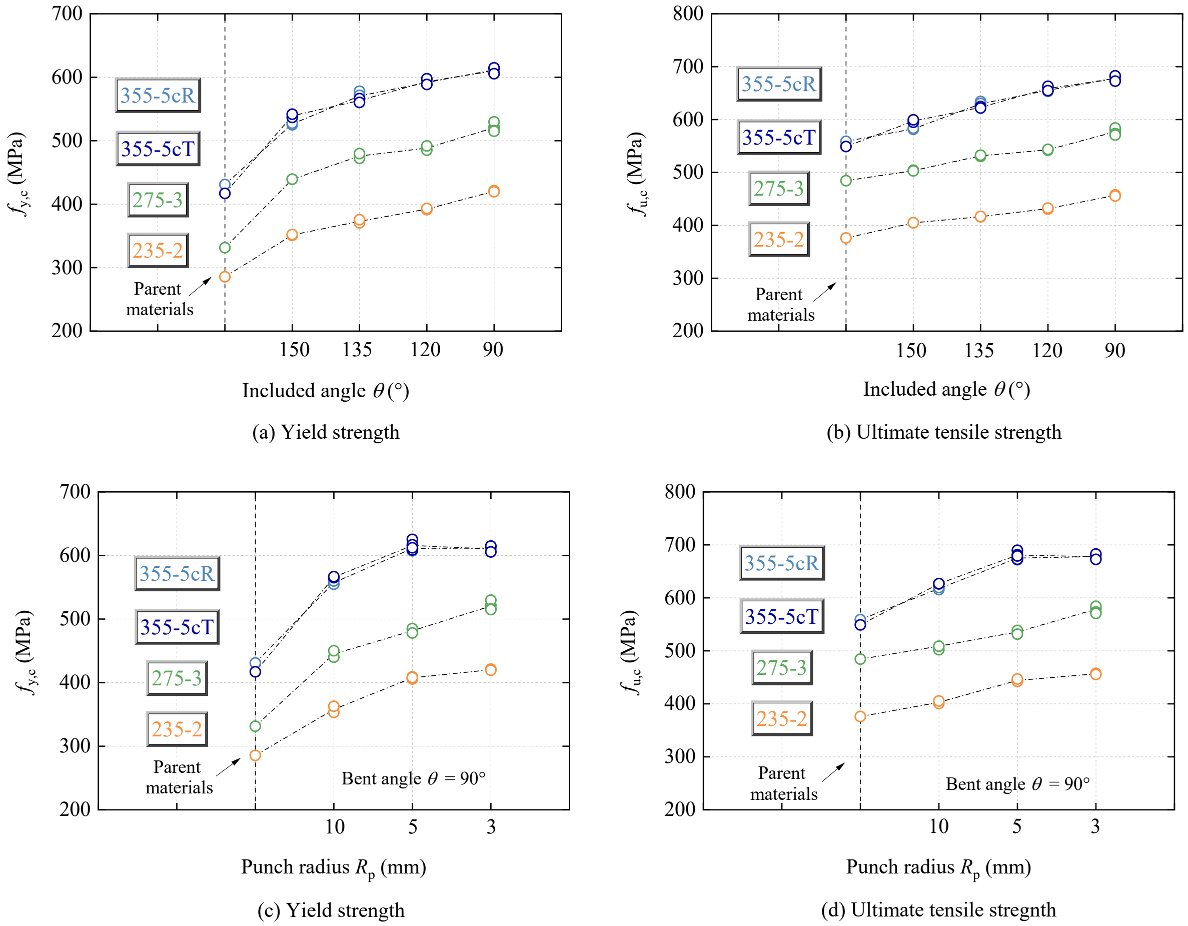

Fig. 10. Trends of the yield strengths $f_{y,c}$ and ultimate tensile strengths $f_{u,c}$ against various punch radii R_p and included angles θ.

To indicate the strength enhancement level, all obtained yield strengths of corner coupons $f_{y,c}$ have been normalized by the yield strengths of parent materials $f_{y,f}$, yielding the ratio $f_{y,c}/f_{y,f}$. The $f_{y,c}/f_{y,f}$ is further plotted against the values of r_i/t in Fig. 11 (a). Anticipated trends are observed that a smaller value of r_i/t results in a larger strength enhancement level reflected by a higher value of $f_{u,f}/f_{y,f}$. For the ultimate tensile strength $f_{u,c}$ of corner coupons, a similar trend can be observed as shown in Fig. 11 (b), indicating that the ultimate tensile strength $f_{u,c}$ can be potentially predicted by the values of $f_{u,f}$, $f_{y,f}$, and r_i/t as well like $f_{y,c}$.

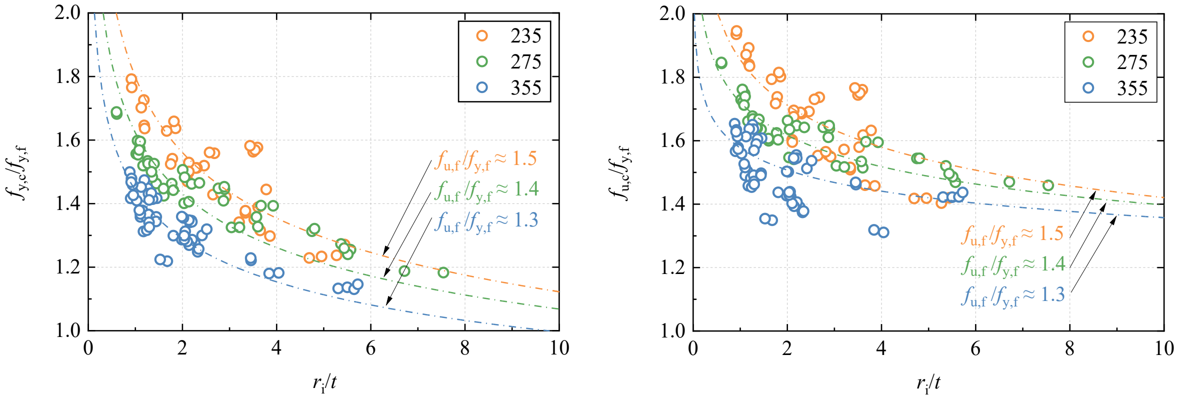

(a) Yield strength (b) Ultimate tensile strength

Fig. 11. Trends of values of $f_{y,c}/f_{y,f}$ and $f_{u,c}/f_{y,f}$ against the inside corner radius to thickness ratios r_i/t.

4.5 Ultimate strain ε_u

The ultimate strains of curved coupons generally decrease with increasing amounts of plastic deformation. The ratios of ultimate strain of corner coupons $\varepsilon_{u,c}$ to ultimate strain of parent materials $\varepsilon_{u,f}$ are plotted against the strength enhancement level. As shown in Fig. 12 (a), a negative correlation exists between the values of $\varepsilon_{u,c}/\varepsilon_{u,f}$ and the values of $f_{y,c}/f_{y,f}$, and the data plots are scattered in the low strength enhancement region, but tight convergence in the relatively high strength enhancement region.

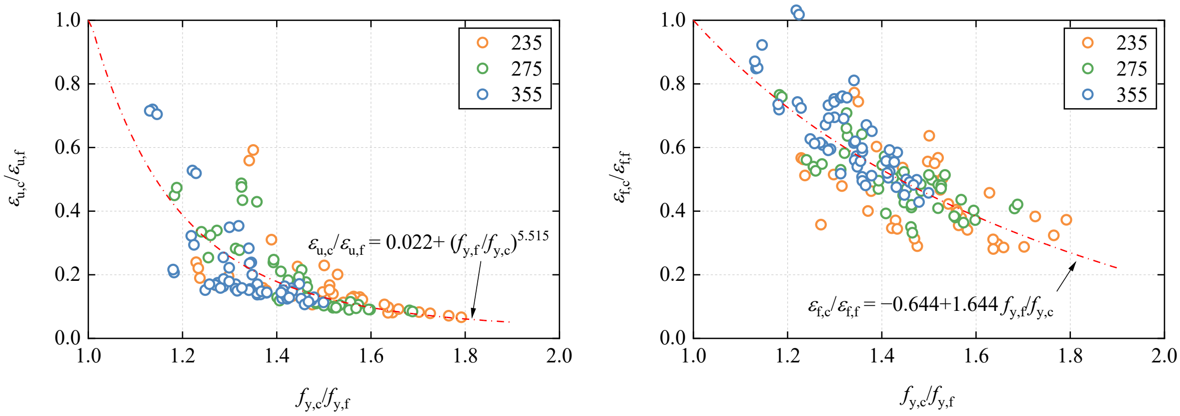

(a) Ultimate strain (b) Elongation at fracture

Fig. 12. Trends of values of $\varepsilon_{u,c}/\varepsilon_{u,f}$ and $\varepsilon_{f,c}/\varepsilon_{f,f}$ against the strength enhancement levels $f_{y,c}/f_{y,f}$.

4.6 Elongation at fracture ε_f

The elongation at fracture ε_f is a reflection of ductility at which level of deformation steels can undergo before fracture. It is should be noted that the test results of elongation at fracture are all larger than 10% for corner coupons tested in this study, even for the corner coupon with the highest strength enhancement level having a $f_{y,c}/f_{y,f}$ of 179%. Following the same data processing method of ε_u, the elongation at fracture of corner coupons $\varepsilon_{u,c}$ is normalized by the elongation at fracture of parent materials $\varepsilon_{u,f}$, and plotted against the strength enhancement level in Fig. 12 (b). Also, a negative correlation can be found between values of $\varepsilon_{f,c}/\varepsilon_{f,f}$ and values of $f_{y,c}/f_{y,f}$.

5. Proposed predictive models

5.1 General

In this section, the experimental results generated in this study together with test data collected from the existing literature were used to form a fundamental database. In total, 379 tensile coupon test results including 137 flat coupons [10, 33-35] and 242 corner coupons [10, 20, 33, 36-42] have been collected. Predictive models for material properties of cold-formed steels were established on the basis of the test database. The flat coupons considered in the database were extracted either from structural steel sheets or flat portions of structural sections that have not experienced cold–works, while the corner coupons were extracted from corner regions of cold-formed square hollow sections (SHS), rectangular hollow sections (RHS), octagonal hollow sections (OctHS), angle sections, and channel sections. The test results in the database cover a wide range of parameters: the measured yield strength of flat coupons $f_{y,f}$ ranging from 232 MPa to 467 MPa, measured yield strength of cold–formed regions $f_{y,c}$ varying from 343 MPa to 680 MPa with corresponding yield strength of parent materials ranging from 256 MPa to 497 MPa, and the value of r_i/t varying from 0.57 to 7.54. Table 4 summarizes the information of collected corner coupon data, including the references, the range of yield strength f_y, the range of r_i/t, and the number of available data. It should be noted that only the tests reporting the values of $f_{y,f}$, $f_{u,f}$, $f_{y,c}$, and r_i/t were included in the database.

Table 4. Summary of details and number of cold-formed corner coupon test data.

References	Range of $f_{y,f}$	Range of $f_{y,c}$	Range of r_i/t	Number of data
–	MPa	MPa	–	–
Key et al. [30]	370-425	451-551	1.50	11
Wilkinson and Hancock [31]	370-457	445-570	0.57-1.41	51
Guo et al. [32]	256-261	343-389	1.11-1.61	6
Gardner et al. [16]	361-482	442-534	0.52-1.74	5
Afshan et al. [33]	363-421	528-608	0.73-1.56	8
Kyvelou et al. [34]	484-497	573-574	0.99-2.32	2
Zhu et al. [35]	476-478	675-680	1.50-1.52	4
Tayyebi and Sun [36]	344-409	553-601	0.78-1.50	5
Liu et al. [27]	381-433	613-661	1.04-1.20	8
This study	286-431	351-625	0.60-7.54	144
			Total:	242

5.2 Material coefficient k and strain–hardening exponent n_{se}

A total of 81 full-range stress-strain curves of parent materials generated in this study and 56 test results from literature were collected to establish predictive models for the material coefficient *k* and the strain–hardening exponent n_{se}. In Fig. 13, the values of $k/f_{y,f}$ and n_{se} are respectively plotted against the values of $f_{u,f}/f_{y,f}$. Good approximations for k/f_y and n_{se} are found against the values of $f_{u,f}/f_{y,f}$, and Eq. (10) and Eq. (11) can be obtained through the linear regression analysis.

$$k = 2.541 f_{u,f} - 1.205 f_{y,f} \tag{10}$$

$$n_{se} = 0.207 f_{u,f} / f_{y,f} - 0.098 \tag{11}$$

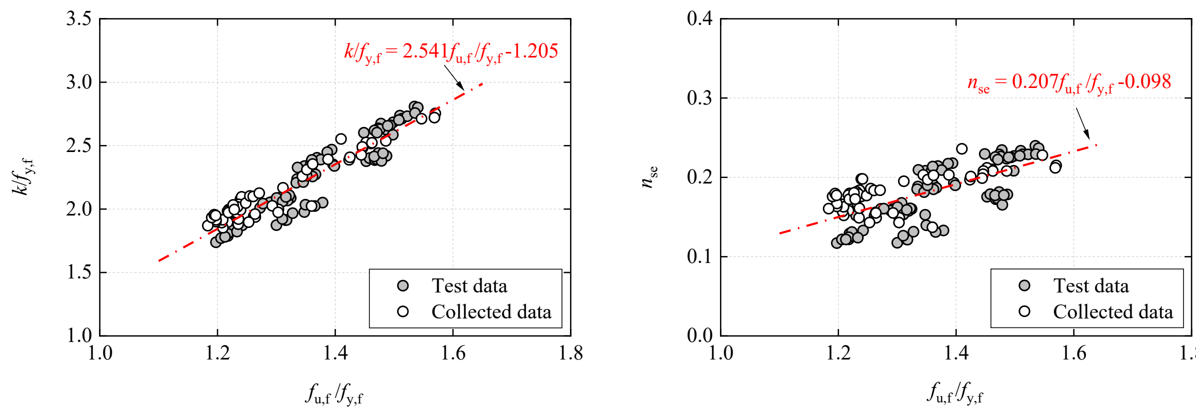

(a) Material coefficient k (b) Strain hardening exponent n_{se}

Fig. 13. Assessment of the material coefficients k and strain hardening exponents n_{se}.

As shown in Table 5, proposed predictive models of k and n_{se} produce reasonable predictions with mean values of 1.00 and 1.02, and corresponding coefficients of variation (CoV) of 0.05 and 0.15, respectively. It is worth noting that the proposed models cover a wider range of material properties than those in Karren [10], and yield more accurate and less scattered predictions as compared to Karren's model expressed in Eq. (2) and Eq. (3). In the following section, Eq. (10) and Eq. (11) are the key components to derive predictive strength enhancement models for the yield strength $f_{y,c}$ and the ultimate tensile strength $f_{u,c}$ of cold–formed corners.

Table 5. Comparison results of parameters using different predictive models.

Parameters	No. of data	The average ratio of predicted to test values

–	–		Proposed model	Karren's model	Gardner's model
k	137	Mean	1.00	1.00	–
		CoV	0.04	0.05	–
n_{se}	137	Mean	1.02	1.03	–
		CoV	0.13	0.15	–
$f_{y,c}$	242	Mean	1.00	1.08	0.91
		CoV	0.06	0.08	0.12
$f_{u,c}$	232	Mean	1.00	–	–
		CoV	0.05	–	–
$\varepsilon_{u,c}$	144	Mean	1.10	–	–
		CoV	0.31	–	–
$\varepsilon_{f,c}$	144	Mean	1.02	–	–
		CoV	0.19	–	–

5.3 Strength enhancement model for $f_{y,c}$

To propose the strength enhancement model for the yield strength $f_{y,c}$ of cold–formed corners, a substantial database comprising 144 test data from this study and 98 collected data from the literature has been established. For some of the experimental data collected from cold–rolled structural hollow sections, the material properties of flat coupon extracted from the flat surface were taken as the benchmark parameters of parent materials, when those of parent materials have not been reported. This approach is deemed reasonably appropriate as the strength enhancement of the flat surface of cold–rolled structural hollow sections is typically relatively small, with an average increasing value of around 4% [20].

To calibrate the coefficients in Karren's model given in Eq. (6), Eq. (6) was rearranged as Eq.(12), in which k and n_{se} can be obtained through Eq. (10) and Eq. (11), and C_1–C_4 are model coefficients. Least square regression analysis was carried out against the collected database, the constant values of C_1–C_4 were then determined as C_1 = 0.873, C_2 = -1.104, C_3 = -0.171, and C_4 = 1.519. The proposed strength enhancement model for $f_{y,c}$ of cold–formed corners can be rewritten as Eq. (13).

$$f_{y,c} = \frac{k\alpha}{(r_i/t)^{\beta}} \text{ in which } \begin{cases} \alpha = C_1 + C_2 n_{se} \\ \beta = C_3 + C_4 n_{se} \end{cases} \tag{12}$$

$$f_{y,c} = \frac{B_c f_{y,f}}{(r_i/t)^{\beta}} \text{ in which } \begin{cases} B_c = 2.769\left(f_{u,f}/f_{y,f}\right) - 0.581\left(f_{u,f}/f_{y,f}\right)^2 - 1.182 \\ \beta = 0.314\left(f_{u,f}/f_{y,f}\right) - 0.320 \end{cases} \tag{13}$$

The accuracy of proposed model was statistically evaluated against the collected database, while the mean value and CoV for the ratio of predicted to measured enhanced yield strengths are 1.00 and 0.06, respectively. As can be found from Fig. 14 (a), the data points are evenly distributed along the fitting line, with the majority of data points falling within ±10% of the predicted values. Also, the prediction accuracy of the proposed model was compared to the models proposed by Karren [10], and Gardner et al. [20] in Fig. 14 (b). Table 5 lists the corresponding mean value and CoV for these three models. In general, the proposed model produces the most accurate and least scattered predictions, while Gardner's and Karren's models tend to underestimate and overestimate the strength enhancement respectively. This discrepancy might be attributed to the different databases used in these studies. It is worth noting that the database used in this study covers widest range of parameters among these studies.

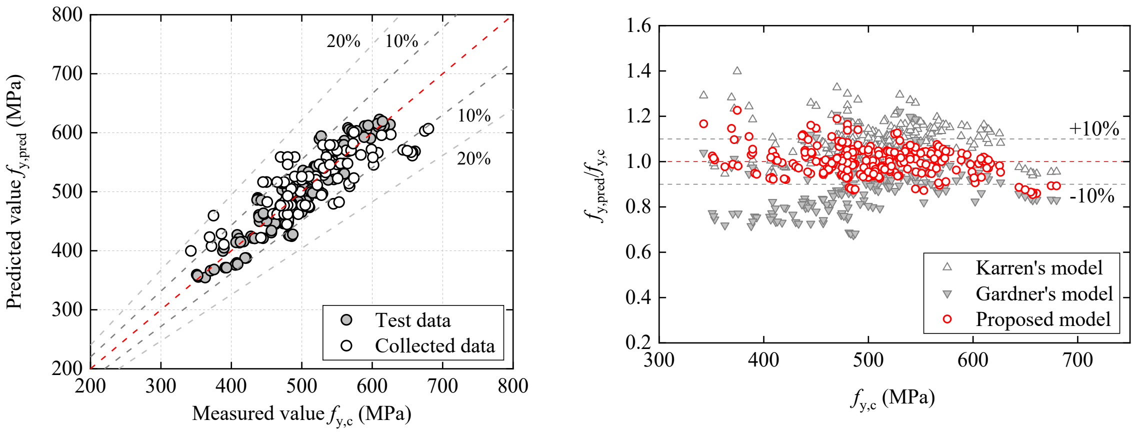

(a) Prediction accuracy (b) Comparisons between different models

Fig. 14. Assessment of the prediction accuracy for enhanced yield strengths in cold-formed corners.

5.4 Strength enhancement model for $f_{u,c}$

As indicated in Fig. 11 (b), a similar trend of enhanced ultimate tensile strength $f_{\mathrm{u,c}}$ against r_{i}/t can be observed. Since not all $f_{\mathrm{u,c}}$ values were reported in the literature, a sub-set of database which has a total of 232 datapoints was established. A modified model adopting the same generalized format as Eq. (12) was adopted, and a series of model coefficients were then determined based on the regression analysis (C_1 = 0.916, C_2 = -0.961, C_3 = -0.145, and C_4 = 1.228). Eq. (14) can be finally obtained to predict $f_{\mathrm{u,c}}$ of cold–formed corners.

$$f_{\mathrm{u,c}} = \frac{B_{\mathrm{c}} f_{\mathrm{y,f}}}{\left(r_{\mathrm{i}}/t\right)^{\beta}} \text{ in which } \begin{cases} B_{\mathrm{c}} = 2.807\left(f_{\mathrm{u,f}}/f_{\mathrm{y,f}}\right) - 0.505\left(f_{\mathrm{u,f}}/f_{\mathrm{y,f}}\right)^2 - 1.217 \\ \beta = 0.254\left(f_{\mathrm{u,f}}/f_{\mathrm{y,f}}\right) - 0.265 \end{cases} \tag{14}$$

As shown in Fig. 15, the proposed model can well predict the enhanced ultimate tensile strength $f_{\mathrm{u,c}}$, yielding a mean predicted to measured ratio and CoV of 1.00 and 0.05, respectively.

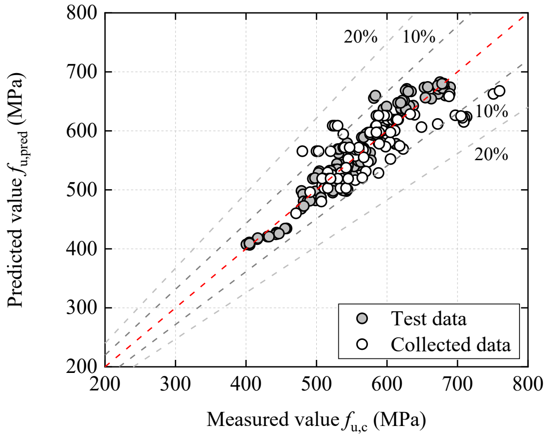

Fig. 15. Assessment of the prediction accuracy for enhanced ultimate tensile strengths in cold-formed corners.

5.5 Ultimate strain $\varepsilon_{u,c}$ and elongation at fracture $\varepsilon_{f,c}$

The test results of cold–formed corners in this study have been used to evaluate the empirical relationships of $\varepsilon_{\mathrm{u,c}}/\varepsilon_{\mathrm{u,f}}$ and $\varepsilon_{\mathrm{f,c}}/\varepsilon_{\mathrm{f,f}}$ with the strength enhancement level. The proposed predictive equations are given in Eq. (15) and Eq. (16), and depicted in Fig. 12.

$$\varepsilon_{u,c}/\varepsilon_{u,f} = 0.022 + (f_{y,f}/f_{y,c})^{5.515} \quad (15)$$

$$\varepsilon_{f,c}/\varepsilon_{f,f} = -0.644 + 1.644 f_{y,f}/f_{y,c} \quad (16)$$

Although the data point is somewhat scattered, the reduced trend of $\varepsilon_{u,c}$ and $\varepsilon_{f,c}$ with the increasing $f_{y,c}/f_{y,f}$ can be reasonably captured by adopting the proposed models, with the mean value of predicted to measured ratios being 1.10 and 1.02, and moderate CoV of 0.31 and 0.19, respectively. It is worth noting that the predicted curve for $\varepsilon_{u,c}$ has been manually biased away from the high concentrations of data that lie between the range of $f_{y,c}/f_{y,f}$ from 1.30 to 1.50 to maintain a reasonable trend, therefore leading to an unconservative prediction ratio of 1.10.

6. Conclusion

A comprehensive investigation into the cold–forming effect of conventional steel has been presented herein. Nine conventional structural steel plates with three nominal grades and three different thicknesses were press–braked into the cold–formed angle sections. Tensile test results on 81 flat coupons extracted from parent materials and 144 corner coupons sectioned from the cold-formed corner region of angle sections were combined with the collected database to establish predictive models to calculate the enhanced yield strength, ultimate tensile strength, ultimate strain and elongation at fracture of cold-formed steels. According to the analysis results, following conclusions can be drawn:

(1) The calibrated predictive equations for material coefficient k and strain–hardening exponent n_{se} were modified based on the test results and collected test data, and slight improvement in prediction accuracy and reduced scatter of prediction value were achieved.

(2) As compared with Karren's original model, the generalized model with the new proposed model

coefficients can provide a more accurate prediction of the enhanced yield strength.

(3) Utilizing the same generalized model for enhanced yield strength, the enhanced ultimate tensile strength can be also accurately predicted, with only the model coefficients being modified.

(4) Equations for predicting the ultimate strain and elongation at fracture were established based on experimental results.

It should be noted that proposed predictive models in this study are applicable to the conventional steels when the actual yield strength of parent materials $f_{y,f}$ ranges from 256 MPa to 497 MPa, the r_i/t value ranges from 0.57 to 7.54.

Conflicts of interest

None.

Acknowledgements

The research work presented in this paper was supported by the Research Grants Council of the Hong Kong Special Administrative Region, China (Project No. 15217119). Financial support from Chinese National Engineering Research Centre for Steel Construction (Hong Kong Branch) was also greatly appreciated.

References

[1] M. Elchalakani, X.L. Zhao, R. Grzebieta, Bending tests to determine slenderness limits for cold-formed circular hollow sections, Journal of Constructional Steel Research 58(11) (2002) 1407-1430.

[2] M. Sun, J.A. Packer, Direct-formed and continuous-formed rectangular hollow sections — Comparison of static properties, Journal of Constructional Steel Research 92 (2014) 67-78.

[3] H.-X. Liu, H. Fang, J.-Y. Zhu, T.-M. Chan, Numerical investigation on the structural performance of octagonal hollow section columns, Structures, Elsevier, 2021, pp. 3257-3267.

[4] A. Godat, F. Legeron, D. Bazonga, Stability investigation of local buckling behavior of tubular polygon columns under concentric compression, Thin-Walled Structures 53 (2012) 131-140.

[5] B. Young, Tests and design of fixed-ended cold-formed steel plain angle columns, Journal of structural engineering 130(12) (2004) 1931-1940.

[6] J. Ye, I. Hajirasouliha, J. Becque, Experimental investigation of local-flexural interactive buckling of cold-formed steel channel columns, Thin-Walled Structures 125 (2018) 245-258.

[7] Q.-Y. Li, B. Young, Tests of cold-formed steel built-up open section members under eccentric compressive load, Journal of Constructional Steel Research 184 (2021) 106775.

[8] Y. Lu, T. Zhou, W. Li, H. Wu, Experimental investigation and a novel direct strength method for cold-formed built-up I-section columns, Thin-Walled Structures 112 (2017) 125-139.

[9] H.D. Craveiro, R. Rahnavard, L. Laím, R.A. Simões, A. Santiago, Buckling behavior of closed built-up cold-formed steel columns under compression, Thin-Walled Structures 179 (2022) 109493.

[10] K.W. Karren, Corner properties of cold-formed steel shapes, Journal of the Structural Division 93(1) (1967) 401-432.

[11] H.G. Rasmussen KJR, Design of cold-formed stainless steel tubular members. I:columns, Journal of Structural Engineering 119(8) (1993) 2349–2367.

[12] D. Dubina, V. Ungureanu, R. Landolfo, Design of cold-formed steel structures, ECCS – European Convention for Constructional Steelwork, 2012.

[13] CEN, Eurocode 3 - Design of steel structures - Part 1-3: General rules - Supplementary rules for cold-formed members and sheeting, European Committee for Standardization, Brussels, 2006.

[14] AISI, AISI S100-16. North American Specification for the Design of Cold-Formed Steel Structural Members, American Iron and Steel Institute, The United States, 2016.

[15] G. Van den Berg, P. Van der Merwe, Prediction of corner mechanical properties for stainless steels due to cold forming, Eleventh International Speciality Conference on Cold-Formed Steel Structures, St. Louise, Missouri, USA, 1992, pp. 571–86.

[16] J. Coetsee, P. Van der Merwe, G. van den Berg, The effect of workhardening and residual stresses due to cold work of forming on the strength of cold-formed stainless steel lipped channel sections, Tenth International Speciality Conference on Cold-Formed Steel Structures, St. Louis, Missouri, USA, 1990, pp. 143–62.

[17] M. Ashraf, L. Gardner, D. Nethercot, Strength enhancement of the corner regions of stainless steel cross-sections, Journal of Constructional Steel Research 61(1) (2005) 37-52.

[18] R.B. Cruise, L. Gardner, Strength enhancements induced during cold forming of stainless steel sections, Journal of Constructional Steel Research 64(11) (2008) 1310-1316.

[19] N. Abdel-Rahman, K. Sivakumaran, Material properties models for analysis of cold-formed steel members, Journal of Structural Engineering 123(9) (1997) 1135-1143.

[20] L. Gardner, N. Saari, F. Wang, Comparative experimental study of hot-rolled and cold-formed rectangular hollow sections, Thin-Walled Structures 48(7) (2010) 495-507.

[21] B. Rossi, S. Afshan, L. Gardner, Strength enhancements in cold-formed structural sections — Part II: Predictive models, Journal of Constructional Steel Research 83 (2013) 189-196.

[22] C.H. Pham, H.N. Trinh, G. Proust, Effect of manufacturing process on microstructures and mechanical properties, and design of cold-formed G450 steel channels, Thin-Walled Structures 162 (2021).

[23] J.-z. Liu, H. Fang, T.-M. Chan, Experimental investigations on material properties and stub column behaviour of high strength steel irregular hexagonal hollow sections, Journal of Constructional Steel Research 196 (2022).

[24] A. Chajes, S. Britvec, G. Winter, Effects of cold-straining on structural sheet steels, Journal of the Structural Division 89(2) (1963) 1-32.

[25] W.F. Hosford, Iron and Steel, Cambridge: Cambridge University Press.2012.

[26] Y. Yang, B. Zhang, Y. Wang, Z. Jiang, K. Li, Mechanical behaviors and constitutive model of structural steel influenced by strain aging, Journal of Constructional Steel Research 192 (2022) 107211.

[27] AS/NZS, AS/ NZS 4600:2018, Cold-formed steel structures, Standards Australia limited, Australia, 2018.

[28] CEN, EN ISO 6892-1:2019. Metallic materials — Tensile testing Part 1: Method of test at room temperature, European Committee for Standardization, Brussels, 2019.

[29] J. Chen, T.-M. Chan, Material properties and residual stresses of cold-formed high-strength-steel circular hollow sections, Journal of Constructional Steel Research 170 (2020).

[30] J. Liao, X. Xue, M.-G. Lee, F. Barlat, G. Vincze, A.B. Pereira, Constitutive modeling for path-dependent behavior and its influence on twist springback, International Journal of Plasticity 93 (2017) 64-88.

[31] J. Lin, Y. Hou, J. Min, H. Tang, J.E. Carsley, T.B. Stoughton, Effect of constitutive model on springback prediction of MP980 and AA6022-T4, International Journal of Material Forming 13 (2020) 1-13.

[32] S. Vitzthum, J.R. Kornmeier, M. Hofmann, M. Gruber, R. Norz, E. Maawad, J. Mendiguren, W. Volk, In-situ analysis of the elastic-plastic characteristics of high strength dual-phase steel, Materials Science and Engineering: A 857 (2022) 144097.

[33] H. Liu, H. Jiang, Y.-F. Hu, T.-M. Chan, K.-F. Chung, Structural behaviour of Q355 and Q460 press-braked rectangular hollow section stub columns, Journal of Constructional Steel Research 197 (2022) 107497.

[34] J. Chen, T.-M. Chan, Experimental assessment of the flexural behaviour of concrete-filled steel tubular beams with octagonal sections, Engineering Structures 199 (2019) 109604.

[35] J. Chen, T.-M. Chan, R.K.L. Su, J.M. Castro, Experimental assessment of the cyclic behaviour of concrete-filled steel tubular beam-columns with octagonal sections, Engineering Structures 180 (2019) 544-560.

[36] P.W. Key, S.W. Hasan, G.J. Hancock, Column behavior of cold-formed hollow sections, Journal of Structural Engineering 114(2) (1988) 390-407.

[37] T. Wilkinson, G.J. Hancock, Tests to examine compact web slenderness of cold-formed RHS, Journal of Structural Engineering 124(10) (1998) 1166-1174.

[38] Y.-J. Guo, A.-Z. Zhu, Y.-L. Pi, F. Tin-Loi, Experimental study on compressive strengths of thick-walled cold-formed sections, Journal of Constructional Steel Research 63(5) (2007) 718-723.

[39] S. Afshan, B. Rossi, L. Gardner, Strength enhancements in cold-formed structural sections — Part I: Material testing, Journal of Constructional Steel Research 83 (2013) 177-188.

[40] P. Kyvelou, L. Gardner, D.A. Nethercot, Testing and Analysis of Composite Cold-Formed Steel and Wood−Based Flooring Systems, Journal of Structural Engineering 143(11) (2017) 04017146.

[41] J.-Y. Zhu, T.-M. Chan, B. Young, Cross-sectional capacity of octagonal tubular steel stub columns under uniaxial compression, Engineering Structures 184 (2019) 480-494.

[42] K. Tayyebi, M. Sun, Stub column behaviour of heat-treated and galvanized RHS manufactured by different methods, Journal of Constructional Steel Research 166 (2020) 105910.